1.12 MEASURED AND MODELED WIND FIELDS IN AN URBAN ENVIRONMENT

Yansen Wang*, Chatt Williamson, Giap Huynh, Sam Chang, David Ligon, and Dennis Garvey

U.S. Army Research Laboratory, Adelphi, MD 20783

1. INTRODUCTION

The Joint Urban 2003 (JUT) project, a cooperative undertaking to study turbulent transport and dispersion in the atmospheric boundary layer conducted in Oklahoma City in the summer of 2003, afforded the U.S. Army Research Laboratory (ARL) the opportunity to leverage our measurement capabilities to increase our understanding of turbulent wind in an urban environment. Our measurement campaign is outlined in a companion paper. In this paper we concentrate on the boundary layer winds measured in this environment and compare these observations with wind fields produced by a three-dimensional boundary layer wind model developed at ARL. The model was developed to meet the requirement of rapid real time simulation on a PC platform. The model uses the wind profiles from measurements or a larger scale model together with urban structure data including building locations, shapes, sizes, and heights to produce a high-resolution diagnostic wind field in the domain of interest. Comparisons between the model results and a number of the measurements obtained during the field campaign are described.

2. MODEL DESCRIPTION

To achieve the speed for real time simulation on a PC platform with reasonable accuracy, we have chosen the mass consistent model instead of using the primitive equation approach. The model is based on the mass conservation principle, which eliminates the divergence in a flow field. that is, given a limited number of observations or a coarsely modeled wind field over complex terrain, the wind field is physically interpolated in such way that mass conservation is satisfied. Mathematically, the problem is to minimize the functional (Sasaki, 1970; Sherman, 1978)

$$E(u,v,w,\lambda)=\int_V \begin{bmatrix} \beta_1^2\ (u-u^0)^2+\beta_1^2\ (v-v^0)^2+ \\ \beta_2^2\ (w-w^0)^2+\lambda(\frac{\partial u}{\partial x}+\frac{\partial v}{\partial y}+\frac{\partial w}{\partial z}) \end{bmatrix} dxdydz \qquad (1)$$

where *x*, *y* are the horizontal coordinates, *z* the vertical coordinate, u^0 , v^0 , w^0 the initial observed velocity components, *u*, *v*, *w* the corrected velocity components, λ the Lagrange multiplier, and β_1, β_2 Gauss precision moduli, which are the wind vector partitioning factors in the horizontal and vertical directions respectively. The Euler-Lagrange equations corresponding to equation (1)

$$u=u^0+\frac{1}{2\beta_1^2}\frac{\partial\lambda}{\partial x},\qquad v=v^0+\frac{1}{2\beta_1^2}\frac{\partial\lambda}{\partial y},$$
$$w=w^0+\frac{1}{2\beta_2^2}\frac{\partial\lambda}{\partial z},\qquad \frac{\partial u}{\partial x}+\frac{\partial v}{\partial y}+\frac{\partial w}{\partial z}=0 \qquad (2)$$

subject to the boundary conditions

$$\lambda(u-u^0)=0,\ \ \lambda(v-v^0)=0, \text{ and } \lambda(w-w^0)=0 \qquad (3)$$

This corresponds to either setting λ=0 ("flow through" free boundaries) or requiring the normal component of the flow at the boundary to remain unchanged after the adjustment.The equations (2) can be cast into an equation for the Lagrange multiplier, λ, in terms of the initial conditions, by differentiating the equations for *u*, *v*, and *w*, and substituting the results into the continuity equation to give a Poisson equation (4). The β_1 and β_2 values are assumed to be constants throughout the small domain V. Without altering their physical meaning, let $\alpha=(\beta_1/\beta_2)$ and β_1 =1 so that α represents the adjustment of the vertical component relative to the horizontal components (4).

$$\frac{\partial^2\lambda}{\partial x^2}+\frac{\partial^2\lambda}{\partial y^2}+\alpha^2\frac{\partial^2\lambda}{\partial z^2}=-2\left(\frac{\partial u^0}{\partial x}+\frac{\partial v^0}{\partial y}+\frac{\partial w^0}{\partial z}\right) \qquad (4)$$

The λ value in equation (4) can be solved numerically by setting the boundary conditions on all facets of the computation domain. The *u, v, w* wind components then can be computed from Equation (2) using the λ value solved from Equation (4). The iterative convergence will be the high resolution diagnostic solution for *u, v, w* for the given boundary and coarse initial conditions (observations). At the lateral boundaries λ is set equal to zero to allow "flow through" in the flow adjustment. At the bottom of the domain "no-flow through" conditions can be satisfied by having the normal derivative vanish, i.e. $\partial\lambda/\partial n$ = 0. A more detailed description of the model (named as 3DSTAT) provided in Wang et al. (2003).

Equation (4) is discretized using a standard 7-point method with second order accuracy in all three spatial directions. The discretization of the Poisson equation in a Cartesian grid leads to a system of linear difference equations. This equation set is non-symmetric, diagonally dominant, and locally dependent on the terrain. Multigrid algorithms are effective and fast in the solution of elliptic equations, and they have recently found many other applications (Briggs et al., 2000). In many cases, the multigrid method is considered the optimal method to solve the elliptical differential equation. Many relaxation

* *Corresponding author address*: Yansen Wang, U.S. Army Research Laboratory, AMSRL-CI-EB, Adelphi, MD 20783-1197; email: ywang@arl.army.mil.

schemes have a smoothing property, such that the high frequency oscillatory modes of the error are eliminated effectively, but lower frequency smooth modes are damped only slowly. The smoothness of the error is relative to the computational grid size, and a smooth mode in a fine grid appears to be high frequency to a coarse grid. The multigrid method takes advantage of this property to speed up the convergence by dealing with the low frequency error in coarser grids. The multigrid method uses coarser grids recursively to relax the smooth mode error and interpolate back to the finer grid. A more detailed numerical implementation of this model using multigrid method is given in Wang et al. (2003). A detailed description of the multigrid method can be found in Briggs et al.(2000). In our comparison test, the multigrid method is about 20 times faster than the traditional Gauss-Seidel relaxation method.

3. OBSERVATION RESULTS

Detailed descriptions about the ARL observation towers and Doppler lidar locations and the sensor setups can be found in a companion paper (Young et al. 2004). The observation results presented here represent a small fraction of the data collected during IOP 4, July 9 of JUT2003. The WindTracer Doppler lidar used in the experiment is a product of Coherent Technologies Inc., Louisville, Colorado. The instrument is operated at wavelength of 2 μm; the pulse repetition frequency is 100Hz, and the gate length is 66 m. The Doppler lidar measures the aerosol backscattering intensity and Doppler shift. These signals are used to retrieve the radial wind speed along the laser beams.

The lidar was located (Fig. 1a) at the northeast side of the Central Business District (CBD). Figure 1b, and Figure 1c are the Planned-position indicator (PPI) and Range-height indicator (RHI) scans respectively around 1527 to 1532 UTC. The wind direction during this time period was from the southwest (210 to 215^{o}). The RHI scan was pointed in 230^{o} clockwise from north, almost parallel to the mean wind direction. The PPI scan was done at a 24.5^{o} elevation angle. Because of the relatively high elevation angle in the PPI scan, the disturbance of the tall buildings in the CBD is not shown in the signal. This makes a good conical scan to construct the Velocity Azimuth Display (VAD) profile (Browning and Wexler, 1968). The atmospheric boundary layer height was about 1.5km because the strong wind condition inhibited the boundary layer growth. The thermal plume effect on the boundary layer growth is limited. The large turbulent structure was also evident at the 0.5 to 1km height in both the PPI and RHI scans. The large turbulent eddies were elongated in the mean wind directions due to the strong wind shear.

ARL tower one was located southwest of CBD in a fairly flat terrain without effect of measurement for the turbulent profiles near the surface. The data from time time period of 1525 to 1530 UTC is analyzed. The wind direction was around 210^{o} , and the mean wind speed were 4.6 and 5.3m/s at 5m and 10m heights respectively.

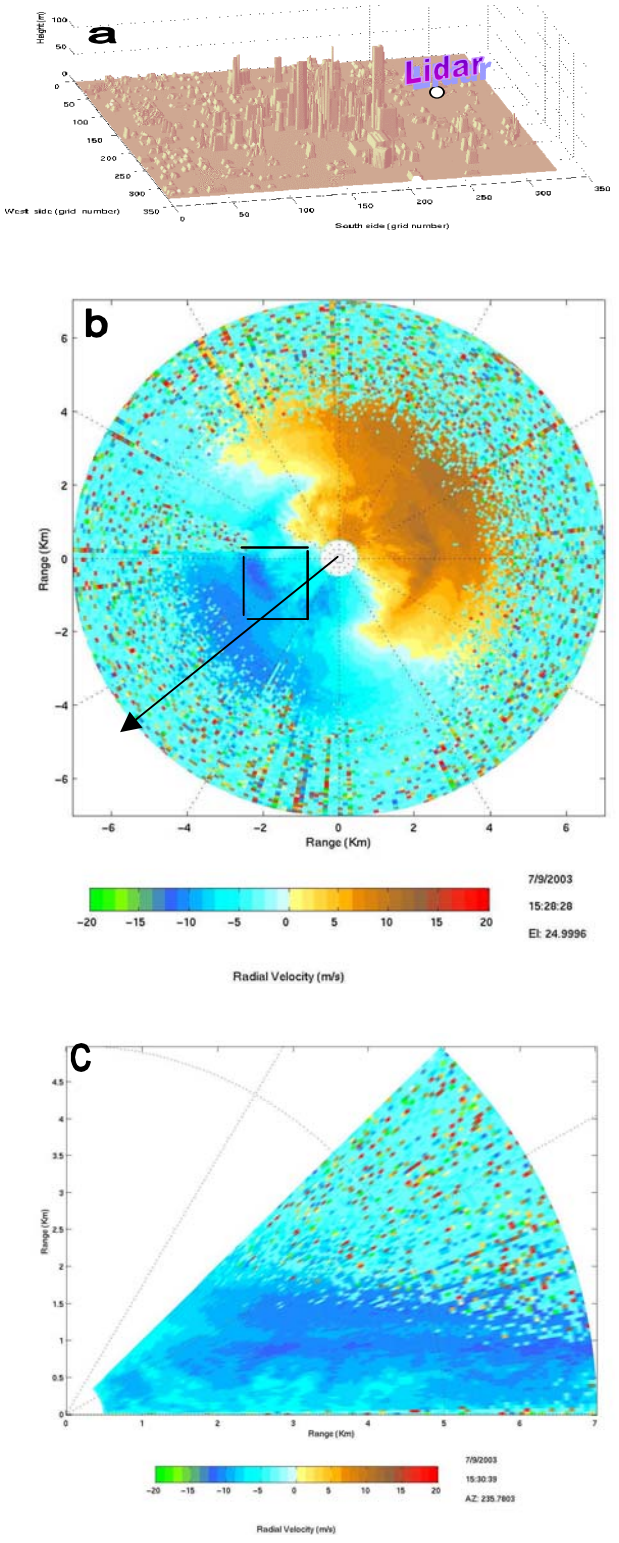

Fig.1 (a) A three-dimensional view of Oklahoma City and location of ARL Doppler lidar; (b) the PPI and (c) RHI scans from Doppler wind lidar around 1530UTC 9 July 2003. The box in (b) shows the position of the CBD relative to the lidar. The arrowed line in (b) shows the azimuth of the RHI scan.

A detailed analysis will be carried out for the lidar and sonic anemometer measurements in a future study. In this paper, we concentrate on the mean flow characteristics to compare with the model simulation.

4. MODEL RESULTS

The 3DSTAT model is used to simulate the wind field in the CBD area. The model domain consists of a 1.6 x 1.6 km area, most part of the CBD. The resolution is 10.6 m in both the x and y directions, and 3m in the vertical. The model grid number is 129 x 129 x 129. The building locations, shapes, and sizes were obtained from a geographical information system, and interpolated to the model grid, and used for the surface morphology or geometry for the model simulation (Fig.1a). The computation for this case takes about 8 minutes CPU time on a dual Pentium 4 linux PC.

As indicated in section 3, the JUT 2003 observation program yielded a rich set of data for model initialization and verification. We have used the VAD wind profile from the ARL lidar at 1527 to 1530 UTC, July 9 as the initial wind above 40 m, and the sonic anemometer wind from ARL tower one for the lower level initial wind. For verification purposes, the 90 m tower data from Lawrence Livermore National Laboratory was used. This tower had 8 sonic anemometers, located at the north side of the CBD.

Figure 2 is the 3DSTAT simulated results using the lidar VAD and sonic anemometer profile as the initial conditions. Fig.2a displays the horizontal wind and Fig.2b shows the vertical wind at z=9m. The mass consistent model showed that mean southwest wind exhibited clockwise turning when approaching a building having east-west orientation. The wind fields around the buildings are modified a great deal. The horizontal wind on the south and north sides of the buildings show significant slow down “shadows”. The mean wind increased considerably in some narrow north-south street canyons. For the locations without buildings, the horizontal wind retained its initial value. The vertical wind distribution (Fig. 2b) shows the upward and downward distribution as expected. The windward side of the buildings had upward motion about 0.2 to 0.5 m/s, while lee side of buildings had downward wind about 0.2 to 0.5 m/s.

Wind profiles from several points of interest are chosen to plot in Fig.3 (see Fig.2b for location). At point 1, the street canyon between the tallest building, Bank One Tower and an adjacent building, the wind speed showed considerable increase due to the Bernoulli effect. Point 2 is located in the lee side of Bank One, and the wind speed had a large reduction compared with the initial profile. Point 3 is located upwind of a building which is about 25m tall. The wind speed was reduced below the building height, but above the building height, the wind speed was larger than other profiles because of the blocking and canyon effect of produced by the building to the east. Points 4 and 5 have no large buildings nearby, and the wind profiles are similar to the initial wind.

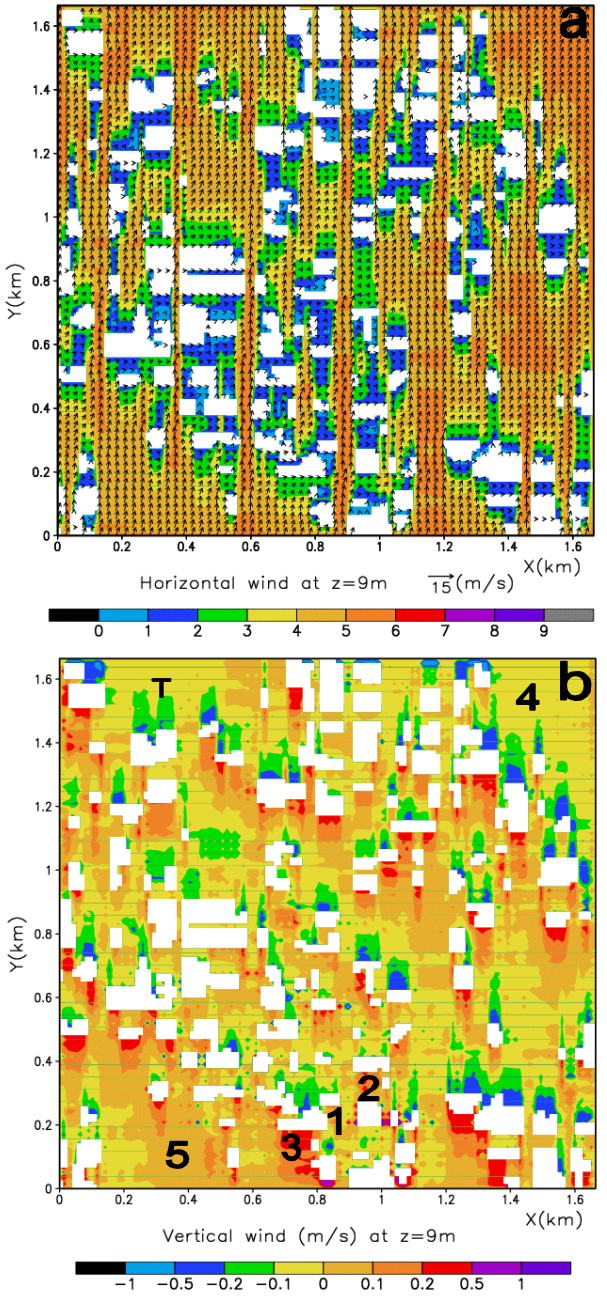

Fig. 2 3DSTAT simulation of the mean wind over CBD, (a) horizontal wind at z=9m. (b) vertical wind distribution at z=9m. **T** in (b) is the location of 90m tower; numbers 1, 2, 3, 4,5 are profile points to be plotted in Fig.3.

The 90m tower located just north of the CBD is used to verify the simulated wind profiles at that location. Fig.4a is a comparison of the simulated wind speed with the observation. The average difference between model and observation results is about 0.7 m/s. The maximum difference is about 1.5 m/s at the 28m height. The wind

speed profile is mostly within the standard deviation of the wind speed during the 5 minutes of observation. The model is generally over predicted wind speed. The wind direction difference between model and observation (Fig.4b) has an average about 8 degree. Wind directions at lower levels are simulated slightly better than upper levels. The 55m and 70m level wind directions had a 15 degree deviation from the observation. The wind speed and direction during 5 minutes had significant variations. Our model uses the 5 minute averaged tower 1 and Doppler lidar VAD wind as the initial wind field, the simulation results is interpreted as the average during this time period.

5. SUMMARY

The JUT 2003 has resulted in a rich data set for the wind flow in an urban domain. We have used the lidar VAD and sonic anemometer wind profile as initial input for the 3DSTAT estimate to simulate the average wind field in the CBD. The wind is quite strong and the thermal effect is minimal in this simulated case. The model performed fairly well for these conditions with systematically over predication in wind speed. We intend to use the JUT 2003 data extensively to validated and perhaps enhance the 3DSTAT model for various wind and stability conditions.

Acknowledgements

We thank Frank Gouveia for providing us the 90m tower sonic anemometer data. We also thank Rob Newsom for producing the Doppler lidar VAD analysis and Ron Calhoun for providing software to read the lidar data.

References

Briggs, W. L., V. E. Henson and S. F. McCormick, 2000: A multigrid tutorial. SIAM publishing. 193pp.

Browning K. A. and R. Wexler, 1968: The determination of kinematic properties of a wind field using doppler radar. *J. Appl. Meteorol.*, 7:105-113.

Sherman, C. A., 1978: A mass-consistent model for wind field over complex terrain. *J. Appl. Meteorol.*, 17:312-319.

Sasaki, Y., 1970: Some basic formalisms in numerical variational analysis. *Mon. Wea. Rev.*, 98:875-883.

Wang, Y., J. J. Mercurio, C. C. Williamson, D. M. Garvey, and S. Chang, 2003: A high resolution, three-dimensional, computationally efficient, diagnostic wind model: Initial development report. U.S. Army Research Laboratory, Adelphi, MD. ARL-TR-3094 (October,2003).

Young Yee, Edward Vidal, Jimmy Yarbrough, Edward Creegan, Scott Elliott, 2003: Wind and Turbulence Observations in Joint Urban 2003. 2004, AMS symposium on planning , nowcasting, and forecasting in urban zone (this volume).

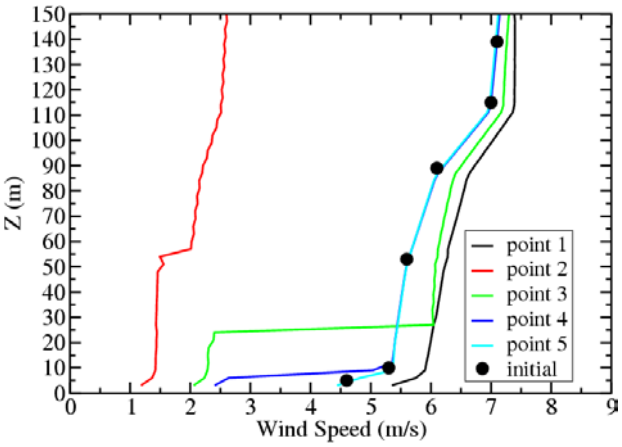

Fig. 3. Horizontal wind profiles from five locations (see Fig. 2b for locations). Notice profiles at points 4 and 5 are same as initial profile at 10 m and up.

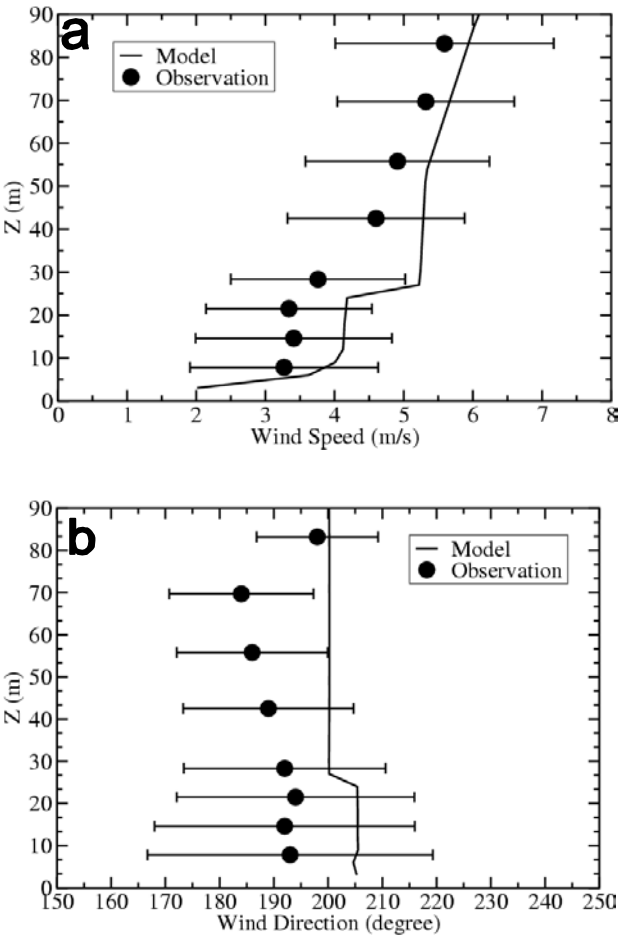

Fig. 4. (a) comparison of the wind profile at the 90 meter tower location; (b) comparison of the wind direction at the 90 meter tower location.